DOI: 10.13009/EUCASS2025-711
11TH EUROPEAN CONFERENCE FOR AERONAUTICS AND SPACE SCIENCES (EUCASS)

DOPPLER RATE-BASED MOTION ESTIMATION OF SURFACE TARGETS USING A SINGLE-CHANNEL SAR CONSTELLATION

*Giulia Pisani**†, Ylenia D'Onofrio*, Pierfrancesco Lombardo* and Debora Pastina**
** Sapienza University of Rome*
Via Eudossiana, 18
Pisani.1883203@studenti.uniroma1.it
† Corresponding Author

Abstract
The exploitation of spaceborne SAR (Synthetic Aperture Radar) constellations to estimate kinematic parameters of moving targets aligns with the recent trend of distributing SAR sensors across several platforms. Here, the spatial diversity granted by an along track constellation of single-channel SAR systems is exploited to estimate the velocity vector of detected maritime targets leveraging the residual Doppler rates simultaneously observed from different view angles. Theoretical performance is derived, analysed both in disturbance free and noisy conditions and compared to simulated analyses. Results show that the spatial diversity provided by the constellation enables the complete velocity estimation with high accuracy.

1. Introduction

Earth observation via spaceborne Synthetic Aperture Radar (SAR) provides a series of advantages thanks to its capability to work all weather and all day. The exploitation of these systems for surface moving targets monitoring is of great interest for several applications in areas such as Homeland Security and Maritime Situational Awareness. Due to SAR imaging working principle, moving targets within SAR images appear shifted and/or smeared due to their motion. Specifically, a radial target velocity component gives rise to an along-track misplacement of the target; an along-track target velocity component determines a variation in the Doppler chirp rate and a consequent mismatch with the parameters used to focus the stationary scene, inducing target smearing. The possibility to estimate the target complete motion (i.e. velocity vector), to refocus the target image and correct the displacement is highly interesting for the considered applications. Different approaches to estimate the mover's kinematic parameters have been studied over the years, though these techniques typically require a multiple channel SAR receiver to estimate the full velocity vector, e.g. [1] for MIMO systems and [2], [3] for a single platform observation using RADARSAT-2 as a reference. A spaceborne dual-platform dual-channel SAR system is instead considered in [6] where the formation is exploited to achieve time diversity with time lag of several seconds between the successive target observations. However, recent year's attention towards miniaturization of space technology has led to the development of a number of large constellations of (single-channel) systems such as Capella Space, [4], ICEYE, [5] etc.: therefore, in this frame, it is of interest to investigate the possibility to estimate the full target motion from the imagery simultaneously acquired by multiple single-channel systems. Among the observables available when using a single-channel SAR system, the Doppler rate has been proven suitable for the retrieval of the target cross-range velocity, e.g [11]. Along this line, a Doppler rate-based full velocity vector estimation technique is here proposed considering a generic formation of N satellites separated in along-track and equipped with single-channel SAR simultaneously observing the same area with squinted geometry. The theoretical performance of the newly proposed technique is derived and analysed both in terms of estimate bias and standard deviation for different acquisition geometries (variations in the squint angle) involving two platforms and different signal to background power ratio (SNR) conditions. These results are obtained by a small errors model and then validated by Monte Carlo simulations. The paper is organized as follows: after introducing the considered acquisition geometry and assumed signal model in Section 2, Section 3 focuses on the new Doppler-based velocity vector estimation technique (Section 3.1) and corresponding theoretical performance (Section 3.2); in Section 4, the performance of the proposed approach is computed according to theory and validated through Monte Carlo simulations. Finally, conclusions are drawn in Section 5.

DOI: 10.13009/EUCASS2025-711

2. Acquisition geometry and signal model

Figure 1a illustrates the reference scenario comprising a constellation of N satellites on the same orbit, evenly spaced by predefined angular separations, and a ship target moving in the acquired scene. The system operates in a SIMO (Single Input, Multiple Output) configuration—only one satellite transmits and receives, while the others are receive-only. To ensure consistent kinematic descriptions, a fixed reference frame is used, independent of each satellite's geometry. A flat Earth model is assumed, with the z-axis perpendicular to the ground plane (x-y), and the x-axis aligned with the along-track direction. The platforms observe the surface mover with coordinates $[x_T(t)\ y_T(t)\ z_T(t)]^T$: particularly, the target is assumed located in the origin at reference time $t_0 = 0$ and characterized by constant velocities along x- and y-axis, specified in equation (1) and shown in Figure 1b detailing the case of N=2 platforms symmetrically positioned with respect to the origin of the reference system.

$$\begin{cases} x_T(t) = V_x t \\ y_T(t) = V_y t \\ z_T(t) = 0 \end{cases} \quad \textbf{(1)}$$

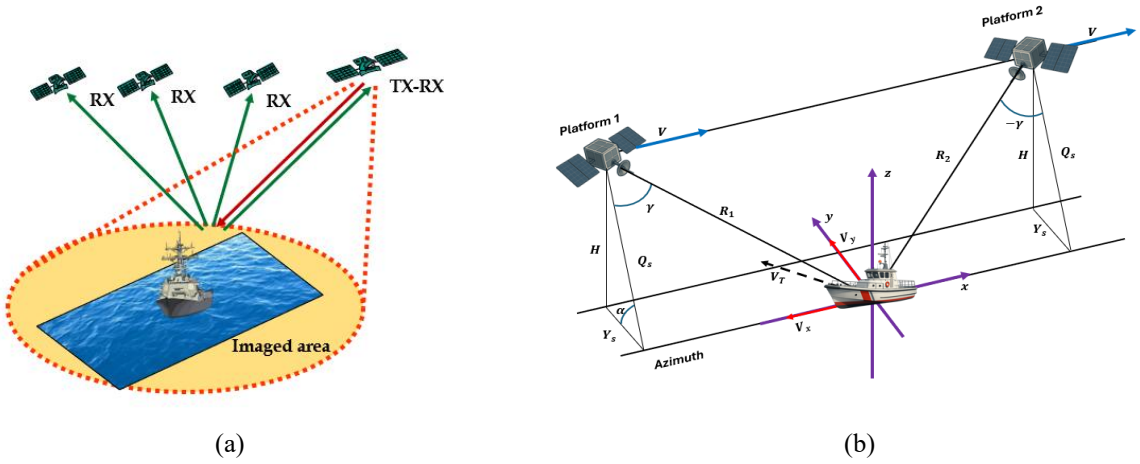

(a) (b)

Figure 1: a) Generic multistatic imaging constellation. b) Acquisition geometry and reference frame.

All platforms in the constellation are assumed to be displaced in along-track (x-axis) while observing the scene with the same grazing angle α, thus all having the same height H and the same Y_s coordinate; each acquisition is characterized by a specific value of the squint angle γ_i, $i = 1, \dots, N$.
To derive the signal model, we start by considering the received signal after range compression and range cell migration correction: the corresponding expression of the mover phase history for the monostatic acquisition (platform 1) is reported in equation (2), while in equation (3) is instead reported the range history as a hyperbolic function of time. Notice that here X_{s1} coincides with the position of satellite 1 at reference time t_0.

$$s_1(t) = \exp\left(-j\frac{4\pi}{\lambda}R_1(t)\right) rect_{T_{az}}(t) \quad \textbf{(2)}$$

$$R_1(t) = \left[(X_{s1} + Vt - V_x t)^2 + \left(Y_s - V_y t\right)^2 + H^2\right]^{\frac{1}{2}} \quad \textbf{(3)}$$

By considering the second order Taylor expansion of the range history at the centre of the synthetic aperture time $t_0 = 0$ we get:

$$\phi_1(t) = \frac{4\pi}{\lambda}R_1(t) \cong \frac{4\pi}{\lambda}(X_{s1}^2 + Y_s^2 + H^2)^{\frac{1}{2}} + 2\pi f_{0T,1} t + \pi \mu_{T,1} t^2 \quad \textbf{(4.1)}$$

$$f_{0T,1} = \frac{2}{\lambda R_1}\left[-Y_s V_y + X_{s1}(V - V_x)\right] \quad \textbf{(4.2)}$$

$$\mu_{T,1} = \frac{2}{\lambda R_1}\left[V_y^2 + (V - V_x)^2\right] - \frac{2}{\lambda R_1^3}\left[-Y_s V_y + X_{s1}(V - V_x)\right]^2 \quad \textbf{(4.3)}$$

DOI: 10.13009/EUCASS2025-711

where equation (4.3) provides the expression of the total Doppler rate of the mover observed by the monostatic system, comprising the motion of both the platform and the mover. Image focusing with respect to the stationary scene compensates a Doppler rate corresponding to equation (4.3) with mover velocities set to zero, namely the rate of the focusing filter is written as

$$\mu_F = \frac{2V^2}{\lambda R_1}\left[1 - \frac{X_{s1}^2}{R_1^2}\right] \tag{5}$$

Thus, after image focusing, the residual Doppler rate due to target uncompensated motion is given by

$$\mu_{res,1} = \frac{2V^2}{\lambda R_1}\left[1 - \frac{X_{s1}^2}{R_1^2}\right] - \frac{2}{\lambda R_1}\left[V_y^2 + (V - V_x)^2\right] + \frac{2}{\lambda R_1^3}\left[-Y_s V_y + X_{s1}(V - V_x)\right]^2 \tag{6}$$

The same analysis can be reiterated for the case of the bistatic acquisition, where the difference from the previous case is given by the fact that the overall expression of the phase will depend on the round-trip signal from platform 1 to the generic platform i, $i = 1, \dots, N$. The expression of the residual rate will thus coincide with the one reported in equation (7). Notice that here the quantity R_i coincides with the distance between platform i and the observed mover at the reference time. This expression of the residual can be used for any other platform operating in SIMO in the constellation, since it refers to a generic bistatic acquisition.

$$\begin{aligned}\mu_{res,i} = \frac{V^2}{\lambda}\left[\frac{1}{R_1}\left(1 - \frac{X_{s1}^2}{R_1^2}\right) + \frac{1}{R_i}\left(1 - \frac{X_{si}^2}{R_i^2}\right)\right] \\ - \frac{1}{\lambda}\left[-\frac{1}{R_i^3}\left(X_{si}(V - V_X) - Y_S V_y\right)^2 + \frac{1}{R_1}\left(V_y^2 + (V - V_x)^2\right) - \frac{1}{R_i^3}\left(X_{si}(V - V_x) - V_y Y_s\right)^2\right. \\ \left. + \frac{1}{R_i}\left((V - V_x)^2 + V_y^2\right)\right]\end{aligned} \tag{7}$$

Above model is exploited in the following section to develop a proper velocity vector estimation technique.

3. Velocity vector estimation technique and theoretical performance

3.1 Doppler rate-based estimation technique

The overall processing chain is sketched in Figure 2 and is organized in two steps: first, the residual Doppler rate is estimated separately for each platform through proper autofocusing techniques ([7], [8]); then, the estimated observables are exploited to estimate the target velocity vector. This work focuses specifically on this second step of the procedure.

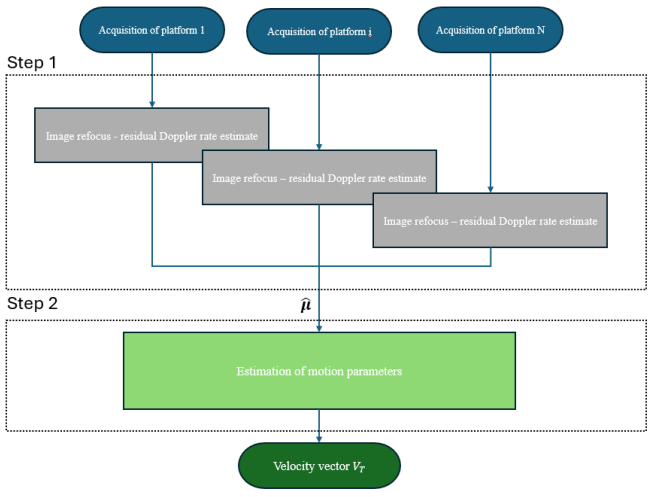

Figure 2: Schematics of the procedure for the velocity estimate.

DOI: 10.13009/EUCASS2025-711

In order to derive the Doppler rate-based estimation technique, first an appropriate linearization of the equation relating the residual Doppler rate and the two velocity vector components V_x and V_y is carried out. Since, in the case of ground moving targets observed by spaceborne SAR systems, it is always true that $V \gg V_x, V_y$, it is possible to neglect the dependency of the residual on the second order terms, thus obtaining the system expression shown in equation (8.1). Equations (8.2) and (8.3) report the expressions of the matrix of the coefficients and both the velocity and Doppler rate residuals vector.

$$\boldsymbol{HV_T} = \boldsymbol{\mu} \tag{8.1}$$

$$\boldsymbol{H} = \begin{bmatrix} \frac{4V^2}{\lambda R_1}\left(1 - \frac{X_{s1}^2}{R_1^2}\right) & -\frac{4V^2}{\lambda R_1^3}(Y_S X_1) \\ \vdots & \vdots \\ -\frac{2V^2}{\lambda}\left[\frac{1}{R_1}\left(\frac{X_{s1}^2}{R_1^2} - 1\right) + \frac{1}{R_i}\left(\frac{X_{si}^2}{R_i^2} - 1\right)\right] & -\frac{2V^2}{\lambda}\left(\frac{X_{s1}Y_S}{R_1} + \frac{X_{si}Y_s}{R_i}\right) \\ \vdots & \vdots \\ -\frac{2V^2}{\lambda}\left[\frac{1}{R_1}\left(\frac{X_{s1}^2}{R_1^2} - 1\right) + \frac{1}{R_N}\left(\frac{X_{sN}^2}{R_N^2} - 1\right)\right] & -\frac{2V^2}{\lambda}\left(\frac{X_{s1}Y_S}{R_1} + \frac{X_{sN}Y_s}{R_N}\right) \end{bmatrix} \tag{8.2}$$

$$\boldsymbol{V_T} = \begin{bmatrix} \boldsymbol{V_x} \\ \boldsymbol{V_y} \end{bmatrix}, \qquad \boldsymbol{\mu} = \begin{bmatrix} \mu_{res,1} \\ \cdot\cdot \\ \mu_{res,N} \end{bmatrix} \tag{8.3}$$

By solving the linear system, an estimate of the velocity vector components can be obtained directly from the measured residual Doppler rates. However, it is important to note that the linearization may introduce estimation errors, which represent the inherent trade-off between model simplicity and accuracy. This specific point is addressed in section 4.

3.3 Theoretical performance

In order to evaluate the accuracy of the velocity estimate in realistic noisy conditions, a small errors model is applied. The theoretical performance is assessed by relating the standard deviations of velocity estimates to those of the residual Doppler rates. Here, the Doppler rate measurements are assumed equal to $\hat{\mu}_{res,i} = \mu_{res,i} + \epsilon_{\mu,i}$, where $\epsilon_{\mu,i}$ is a zero-mean Gaussian random variable whose variance is set equal to the corresponding value of the Cramér-Rao lower bound [9]. Equation (9) expresses this variance, where T_{az} is the synthetic aperture duration, and SNRγ is the Signal-to-Noise Ratio taking into account the platforms' squint angle γ. Specifically, if we denote with SNR the value corresponding to a zero-squint geometry, then we have SNRγ=SNR·(cosγ)^4 to account the additional path involved by squinted geometries.

$$\sigma_{\mu}^2 = \frac{90}{T_{az}^4 SNR_{\gamma} \pi^2} \tag{9}$$

Building on the previous assumptions, the variance of the velocity estimate can be derived as a function of the angular separation between platforms using a small errors framework. In particular, given the approximated linear relationship between the residual Doppler rates and velocity components, the measurement errors map linearly into velocity estimation errors as expressed in Equation (10).

$$\begin{bmatrix} \epsilon_{V_x} \\ \epsilon_{V_y} \end{bmatrix} = (H^T H)^{-1} H^T \begin{bmatrix} \epsilon_{\mu_1} \\ \vdots \\ \epsilon_{\mu_N} \end{bmatrix} \tag{10}$$

Here, $(H^T H)^{-1} H^T$ coincides with the pseudoinverse of matrix H (equal to the inverse when N=2). Since matrix $\boldsymbol{H}$ depends solely on geometric parameters, the derived performance metrics apply to any pair of target velocities. Once the mapping matrix has been assessed, it is thus possible to retrieve the expression of the covariance matrix for the velocity vector, here denoted as $\boldsymbol{C_v}$, by assuming that the Doppler rate measurements from the platforms are uncorrelated, as shown in equation (11):

DOI: 10.13009/EUCASS2025-711

$$\boldsymbol{C_v} = E\left(\begin{bmatrix}\epsilon_{V_x}\\ \epsilon_{V_y}\end{bmatrix}[\epsilon_{V_x} \quad \epsilon_{V_y}]\right) = (H^TH)^{-1}H^TE\left(\begin{bmatrix}\epsilon_{\mu_1}\\ \vdots\\ \epsilon_{\mu_N}\end{bmatrix}[\epsilon_{\mu_1} \cdots \quad \epsilon_{\mu_N}]\right)H(H^TH)^{-1} =$$
$$= (H^TH)^{-1}H^T\begin{bmatrix}\sigma^2_{\mu_1} & \cdots & 0\\ \vdots & \ddots & \vdots\\ 0 & \cdots & \sigma^2_{\mu_N}\end{bmatrix}H(H^TH)^{-1}=(H^TH)^{-1}H^T\boldsymbol{C_\mu}H(H^TH)^{-1} \quad \textbf{(11)}$$

being $\boldsymbol{C_\mu}$ the covariance matrix of the exploited observables. Results in terms of achievable performance are reported in the following section for the specific case of a formation of two platforms.

4. Performance analysis

For the sake of performance assessment and comparison, a typical LEO acquisition geometry is assumed with two platforms (N=2), Figure 1a), and main parameters summarized in Table 1. Here, both platforms are assumed to be operating in squinted StripMap mode, respectively γ for platform 1 and $-\gamma$ for platform 2, where platform 1 (TX-RX) is taken as forward-looking and platform 2 (RX only) is backward-looking.

Table 1: Reference geometric parameters for image acquisition.

Quantity	Value
Height (H)	570 km
Squint angle (γ)	26°
Radence angle (α)	65°
Platform velocity (V)	7.57 km/s
Wavelength (λ)	0.03 m
Antenna aperture (d_{az})	3.4 m

Achievable performance is first analysed by evaluating the impact of the linearization in disturbance free conditions. Figure 3 shows the estimate error on V_x (Figure 3a) and V_y (Figure 3b) for target velocities ranging in the intervals [-10 m/s, 10 m/s] for x-component and [-15 m/s, 15 m/s] for the y-component. Figure 3 shows that, within the velocity range considered well suited for ship targets, the linearization error is negligible compared to the velocity components themselves. Specifically, the maximum error is about 0.02 m/s for $(V_x, V_y) = (\pm 10, \pm 15)$. This confirms that the linearized model is well suited for reliable velocity estimation of the moving target.

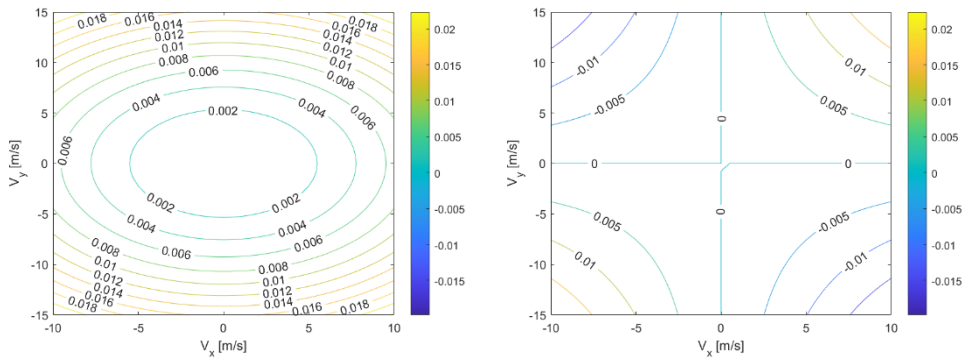

(a) (b)

Figure 3: Linearization error on the estimate for a) velocity component V_x. b) velocity component V_y.

DOI: 10.13009/EUCASS2025-711

Moving to noisy conditions, both the results in terms of theoretical performance and Monte Carlo simulations (10^4 trials) are here provided. In Figures 4a, the behaviour of σ_μ is reported as a function of SNR for a fixed value of $\Delta\gamma = 2\gamma = 52°$ while in Figures 4b the same quantities are reported as a function of $\Delta\gamma$ for a fixed $SNR = 30$ dB. All results are given for a reference value of the target velocity vector equal to $(V_x, V_y) = (10,10)$ m/s resulting in a residual Doppler rate for platform 1 with $\gamma = 26°$ equal to 14.043 Hz/s. The following observations apply: (i) the Cramér-Rao lower bound matches closely with simulations; (ii) increasing SNR improves residual Doppler rate accuracy, as expected; (iii) despite SNRγ decreasing with larger angular separations, the accuracy of residual Doppler rate slightly improves as a consequence of the increase of the synthetic aperture time.

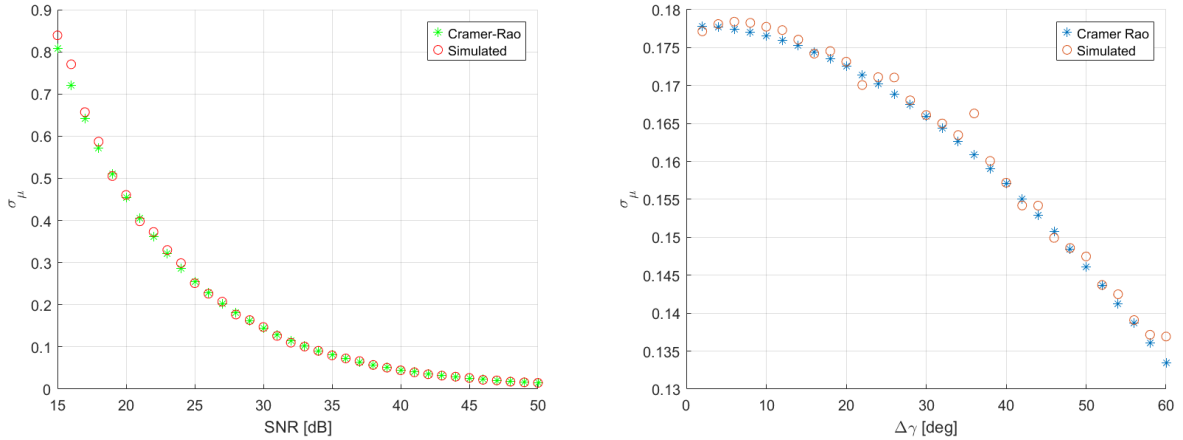

(a) (b)

Figure 4: Standard deviation of the estimate of the residual Doppler rate (a) as a function of SNR for an assigned $\Delta\gamma = 52°$; (b) as a function of $\Delta\gamma$ for a fixed $SNR = 30$ dB.

Figures 5a and 5b show the accuracy of velocity component estimates as a function of the angular separation $\Delta\gamma$ between platforms, for a reference $SNR = 30$ dB. From the provided results, we notice that the accuracy of V_x slightly degrades with increasing $\Delta\gamma$, mainly due to the reduction in SNR_γ. Conversely, the accuracy of V_y improves with larger angular separations, reflecting increased sensitivity of the residual Doppler rate as the squint angle grows. In contrast, when $\Delta\gamma \to 0$ the performance degrades and the standard deviation shows a large increase: this behavior is anyway expected since, when the two platform constellation degenerates in the single platform case, only the along track component (i.e. x-component) can be estimated from the Doppler rate. Finally, Figures 6a and 6b report the bias on both velocity components under noisy conditions across varying $\Delta\gamma$. As evident, the bias on both components remains almost stable and comparable to noise-free results (cf. Figure 4a), regardless of $\Delta\gamma$ value.

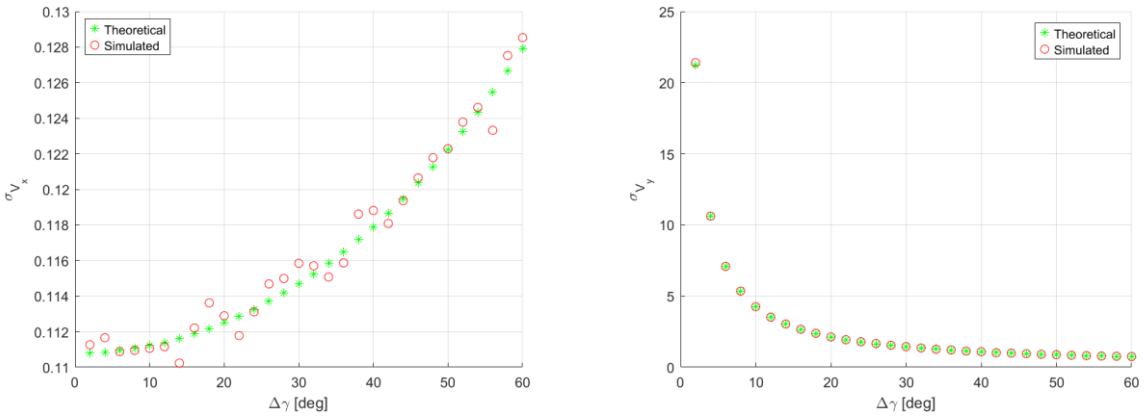

(a) (b)

Figure 5: Standard deviation of the velocity estimate as a function of angular diversity for $SNR = 30$ dB and $(V_x, V_y) = (10,10)$ m/s. a) Accuracy on the estimate of V_x. b) Accuracy on the estimate of V_y.

DOI: 10.13009/EUCASS2025-711

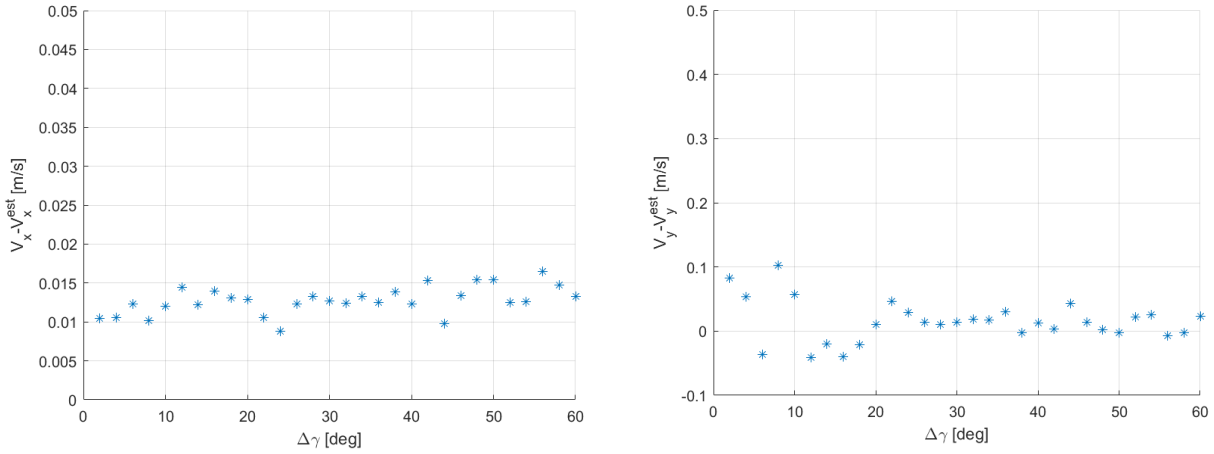

(a) (b)

Figure 6: Bias on the velocity estimate in presence of noise when $SNR = 30$ dB and $(V_x, V_y) = (10,10)$ m/s as a function of $\Delta\gamma$ between platforms. a) Bias on the estimate of V_x. b) Bias on the estimate of V_y.

5. Conclusions

In this article, a technique to estimate the velocity vector of a maritime target has been proposed, based on the estimates of the residual Doppler rates observed in spatial diversity allowed by the constellation. First, the analytical relationship between the residuals and the mover's kinematic parameters has been retrieved for a constellation comprising N (≥ 2) platforms. Then, the proposed velocity vector estimation technique has been derived and the corresponding theoretical performance characterized by deriving the errors covariance matrix. The performance analysis has been carried out both in a disturbance free and a Gaussian-noisy environment for a formation of two satellites (one active and one passive) separated in along-track direction and symmetrically placed with respect to the reference target position. Finally, the theoretical analysis has been validated by Monte-Carlo simulations. Shown results highlight that an increase in the angular separation between the platforms of the constellation will grant a higher quality estimate of the velocity vector. For instance, for $\Delta\gamma = 20°$ and $SNR = 30$ dB the results show $\sigma_{V_x} = 0.11$ m/s, while $\sigma_{V_y} = 2.13$ m/s. By considering instead a larger angular separation, for example $\Delta\gamma = 50°$, the performance in terms of accuracy of V_y will increase ($\sigma_{V_y} = 0.88$ m/s) due to higher sensitivity of the Doppler rate to this component, while V_x remains nearly unchanged ($\sigma_{V_x} = 0.12$ m/s). These results prove that a good accuracy of the velocity estimate can be achieved by properly locating the platforms. Moreover, the performance could be enhanced by considering either a larger number of platforms or additional receiving channels, since this may allow to use other observables such as the along track interferometric phase, as studied in [10].

Acknowledgment

This work has been funded by the project Oceanos, "Monitoring Agricultural and Coastal Marine Areas Using Next-Generation Satellite Technologies", (ARS01_00536), PON "Research and Innovation" 2014 – 2020 Aerospace Sector.

References

[1] D. Pastina P. Lombardo and F. Turin. 2015. Ground moving target detection based on mimo SAR systems. *IEEE JSTARS, Vol 8*.

[2] Cerutti-Maori D. and Sikaneta I. 2013. A generalization of DPCA processing for multichannel SAR/GMTI radars. *IEEE Transactions on Geoscience and Remote Sensing*, vol. 51.

[3] Cerutti-Maori D., Sikaneta I. And Gierull C. H. 2012. Optimum SAR/GMTI processing and its application to the radar satellite RADARSAT-2 for traffic monitoring. *IEEE Transactions on Geoscience and Remote Sensing*.

[4] J. Homssi K. Szczygielska M. Laaninen, M. Neerot and J. Niemczyk. 2022. Iceye radar constellation development and evolution. *14th European Conference on Synthetic Aperture Radar*.

[5] Castelletti D., Farquharson G., Brown J., De S., Yague-Martinez N., Stringham C., Yalla G., Villarreal A. 2022. Capella space first operational SAR satellite. *IGARSS*.

[6] Baumgartner S. V. and Krieger G. 2016. Dual-Platform Large Along-Track Baseline GMTI. *IEEE Transactions on Geoscience and Remote Sensing*, *vol. 54.*

DOI: 10.13009/EUCASS2025-711

[7] Gao, A.; Sun, B.; Yan, M.; Xue, C.; Li, J. 2023. Modified Auto-Focusing Algorithm for High Squint Diving SAR Imaging Based on the Back-Projection Algorithm with Spectrum Alignment and Truncation. *Remote Sens.*

[8] Y. Lou, H. Lin, Q. Chen, M. Xing, S. Zhou and G. -C. Sun. 2024. 2-D Autofocus for High-Squint SAR Based on Affine Coordinate Back-Projection Algorithm. *IEEE Transactions on Geoscience and Remote Sensing, vol. 62, pp. 1-17, no. 5228217.*

[9] S. Peleg and B. Porat. 1991. The Cramer-Rao lower bound for signals with constant amplitude and polynomial phase. *IEEE TRANSACTIONS ON SIGNAL PROCESSING, VOL. 39. NO. 3.*

[10] Y. D'Onofrio, D. Pastina and P. Lombardo. 2025. Surface Targets Velocity Vector Estimation exploiting Constellations of SAR Systems. *11th European Conference for AeroSpace Sciences (EUCASS)*.

[11] D. Pastina, F. Turin. 2015. Exploitation of the COSMO-SkyMed SAR System for GMTI Applications. *IEEE Journal of Selected Topics in Applied Earth Observations and Remote Sensing*, Volume 8, Issue 3.